ACS APPLIED MATERIALS & INTERFACES

Letter

www.acsami.org

Calcium Carbonate Nanoplate Assemblies with Directed High-Energy Facets: Additive-Free Synthesis, High Drug Loading, and Sustainable Releasing

Jing Zhang,[†] Yu Li,[†] Hao Xie,[‡] Bao-Lian Su,[§] Bin Yao,[†] Yixia Yin,[†] Shipu Li,[†] Fang Chen,[∥] and Zhengyi Fu*,[†]

[†]State Key Laboratory of Advanced Technology for Materials Synthesis and Processing and [‡]Department of Biological Science and Biotechnology, Wuhan University of Technology, Wuhan 430070, P.R. China

[§]Laboratory of Inorganic Materials Chemistry, University of Namur, B-5000 Namur, Belgium

[∥]Department of Medicine Experiment, Wuhan General Hospital, Wuhan 430070, P.R. China

Supporting Information

ABSTRACT: Developing drug delivery systems (DDSs) with high drug-loading capacity and sustainable releasing is critical for long-term chemotherapeutic efficacy, and it still remains challenging. Herein, vaterite $CaCO_3$ nanoplate assemblies with exposed high-energy {001} facets have been synthesized via a novel, additive-free strategy. The product shows a high doxorubicin-loading capacity (65%); the best of all the $CaCO_3$-based DDSs so far. Also, the product's sustainable releasing performance and its inhibition of the initial burst release, together, endow it with long-term drug efficacy. The work may shed light on exposing directed high-energy facets for rationally designing of a drug delivery system with long-term efficacy.

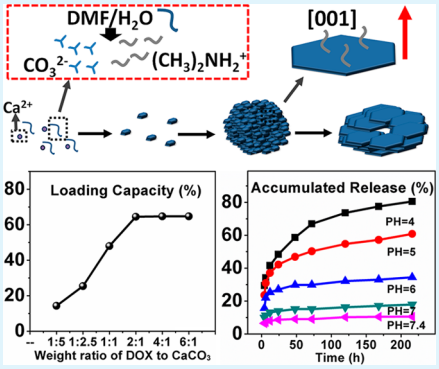

KEYWORDS: *calcium carbonate, nanostructure, additive-free synthesis, drug delivery, high-energy facet*

Developing anticancer drug delivery systems (denoted as DDSs) has become a primary research focus for cancer cure in the past few decades.[1,2] Inorganic-based DDSs, because of their desirable biocompatibility, convenient surface conjugation, and excellent mechanical stability, have been actively pursued.[3−5] A high drug-loading capacity is generally required to attain desirable drug efficacy, and an adequate initial release as well as a subsequent sustained release are also considered critical for long-term pharmacological function, and these have been achieved to some extent, according to a few reports.[6−8] Thus, to design and construct an inorganic-based DDS with both high drug-loading capacity and sustainable releasing behavior via a convenient, low-cost route still remains a challenge.[9,10] Since $CaCO_3$ was proposed as an anticancer drug vehicle in 2008, $CaCO_3$-based DDSs have been demonstrated to be promising candidates because of their intrinsic pH-sensitivity, low-toxicity, and good biocompatibility.[11−14] Nevertheless, to the best of our knowledge, a considerable amount of tested systems based on calcium carbonate feature low drug-loading capacity and lack sustainable release afterward.[11−14] Thus, it is still a challenge to achieve $CaCO_3$-based DDS with high drug-loading capacity and sustainable releasing behavior for practical applications.

For an inorganic carrier, interactions between drug molecules and inorganic surfaces play key roles in drug loading and release. To date, most work has focused on functionalizing inorganic surfaces with particular organic groups to facilitate bonding with drug molecules.[15,16] Though the inherent nature of an inorganic crystal might be of interest in several ways, the useful effects of crystal facets, which have active physicochemical properties, have rarely been demonstrated and highlighted for designing a DDS.[9,17] Thus, we speculate that interactions between coordinatively unsaturated high-energy crystal facets and drug molecules might be favorable for high drug loading and sustainable releasing, because of the crystal's distinct bonding strength.

Additives, such as surfactants, and synthetic polymers are always employed to control the morphology and the polymorph, as well as to aid surface conjugation with organic residues of an inorganic-based carrier.[18,19] However, organic residues on crystal surfaces might be avoidable in further applications, and presently, they hinder use of the effect of the high-energy facets on drug loading and releasing. Alternatively, crystallization in mixed solvents without additives, paves the way for synthesizing inorganic materials with relatively "clean" crystal surfaces.[20] Until now, most work gives full attention to the function of additives in $CaCO_3$ crystallization based on the familiar additive-free systems.[21,22]

Received: June 2, 2015
Accepted: July 10, 2015
Published: July 10, 2015

DOI: 10.1021/acsami.5b04819
ACS Appl. Mater. Interfaces 2015, 7, 15686−15691

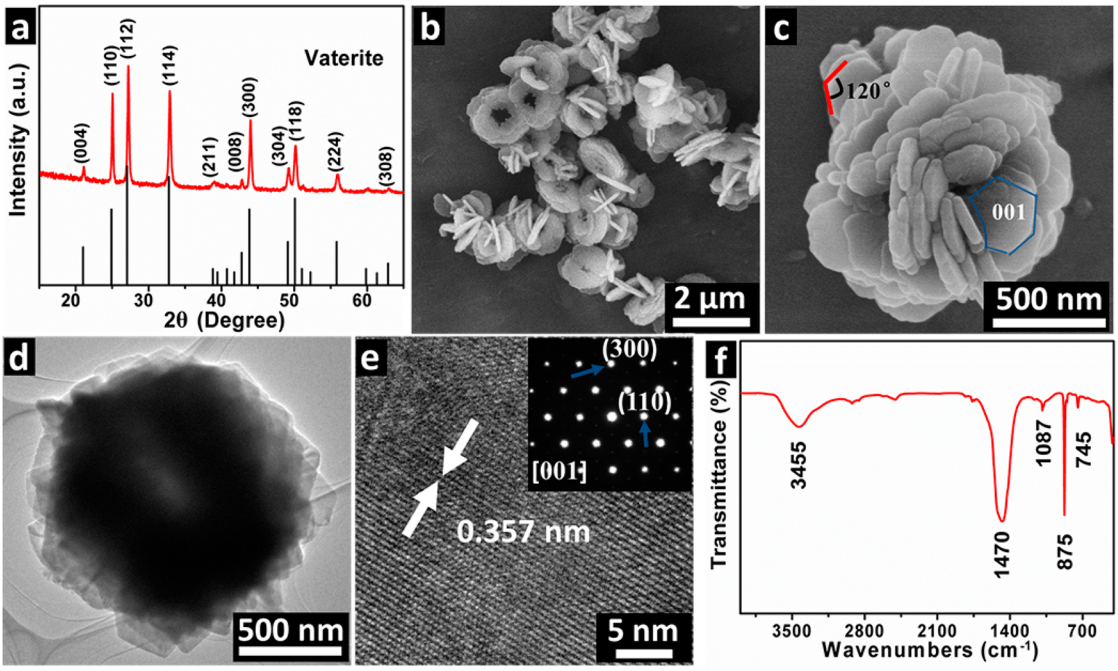

Figure 1. (a) XRD pattern of the vaterite $CaCO_3$ nanoplate assemblies, and standard XRD pattern of vaterite. (b, c) FESEM images, (d) TEM image, and (e) HRTEM image of the vaterite $CaCO_3$ nanoplate assemblies, with SAED pattern inset in e. (f) FT-IR spectrum of the vaterite $CaCO_3$ nanoplate assemblies.

However, these additive-free systems alone usually lack enough morphological and polymorphic control, with products limited to usual morphologies and structures.[22,23] Thus, it is desirable to develop a new additive-free system to obtain $CaCO_3$-based vehicle with directed high-energy crystal facets.

In this work, we propose an additive-free strategy for synthesizing a unique vaterite $CaCO_3$ nanoplate assemblies with exposed, {001} high-energy facets. By employing doxorubicin (DOX) as the model drug molecule, we demonstrate high drug-loading capacity (65%) of our product. Moreover, the inhibition of initial burst release, and the continuous sustainable releasing can be realized for this type of DDS, rendering it a promising candidate for anticancer drug vehicle.

A typical sample is synthesized by solvothermal reaction of $Ca(CH_3COO)_2$ (c = 7 mM) in DMF/H_2O mixed solvent (3:1 v/v) at 120 °C for 6 h. (see the experimental section in the Supporting Information) The structural and morphological characterizations of the typical sample are presented in Figure 1. The XRD pattern (Figure 1a) shows diffraction peaks indexed to vaterite $CaCO_3$ (space group: $P63/mmc$, JCPDS 33−0268). Notably, the single-polymorph nature is distinctly identified as no peaks from calcite or aragonite are detected. As shown from FESEM and TEM images in Figure 1b−d, the as-synthesized sample is characterized by three-dimensionally (3D) assembled nanostructures consisting of stacked nanoplates with a submicronsized cavity near the center. The well-defined and monodispersive $CaCO_3$ nanoplate assemblies are ca. 1.2 μm in diameter and ca. 0.8 μm thick. The nanoplate subunit, roughly 40 nm thick (Figure S1), has hexagonal edges (red marks in Figure 1c), which are ascribed to the hexagonal symmetry of the vaterite polymorph. Figure 1e shows a HRTEM image of the nanoplate subunit with a regular lattice fringe of the {110} planes (d = 0.357 nm), confirming the vaterite polymorph, and the single-crystalline nature of the nanoplate subunit. Moreover, a typical SAED pattern taken from the edge of a nanoplate subunit (inset in Figure 1e) shows single-crystalline-like diffraction spots viewed from the [001] zone axis, confirming the exposed high-energy {001} facets as marked in Figure 1c, which, to the best of our knowledge, have rarely been exposed without the aid of additives.[24−26]

The FT-IR spectrum in Figure 1f shows that the typical absorption bands that correspond to the CO_3^{2-} vibrations of vaterite (CO_3^{2-} bands at 745 cm^{-1}, 875 cm^{-1}, 1088 and 1477 cm^{-1}).[24,25] The weak absorption bands of 2922 cm^{-1} is characteristic absorption of C−H stretching, and 2507 cm^{-1} is likely assigned to the stretching vibration of N−H in R_2-NH_2^+ or R_3-NH^+. Upon heating, TG-DSC curves (Figure S2) show a notably small weight loss of ca. 2.5% below 400 °C, which can be ascribed to adsorbed water, and the organic residues. From the results, we pay attention that, there is a relatively small amount of organic residues left on the crystal surface, compared to previous work.[24,25] Thus, vaterite $CaCO_3$ nanoplate assemblies with large quantities of exposed {001} facets were successfully synthesized by this additive-free route. Compared to previous work, the product herein, features a more suitable particle size, and a larger amount of the exposed {001} facets provided by the assembly of the submicrometer-sized vaterite nanoplates.[24,25]

In our reaction system, multiple roles of the DMF/H_2O solvent are demonstrated, apart from the regular solvent effects of increased supersaturation and decreased ionic mobility and activity. TG-MS curves (Figure 2a, b) show a variety of species released as temperature increases (start at T = 80−90 °C), involving H_2O, CO_2, $(CH_3)_2NCOH$, and $(CH_3)_2NH$. Actually, it is speculated that these moieties contribute to building ions (CO_3^{2-}) for $CaCO_3$ crystallization, crystal modifier ($(CH_3)_2NH_2^+$) for stabilizing vaterite and promoting the high-energy {001} facets formation. It is well recognized that vaterite does not usually expose its high-energy {001} facets, whereas crystal modifier, such as ammonium ions, stearic acid monolayers, etc., have been

DOI: 10.1021/acsami.5b04819
ACS Appl. Mater. Interfaces 2015, 7, 15686−15691

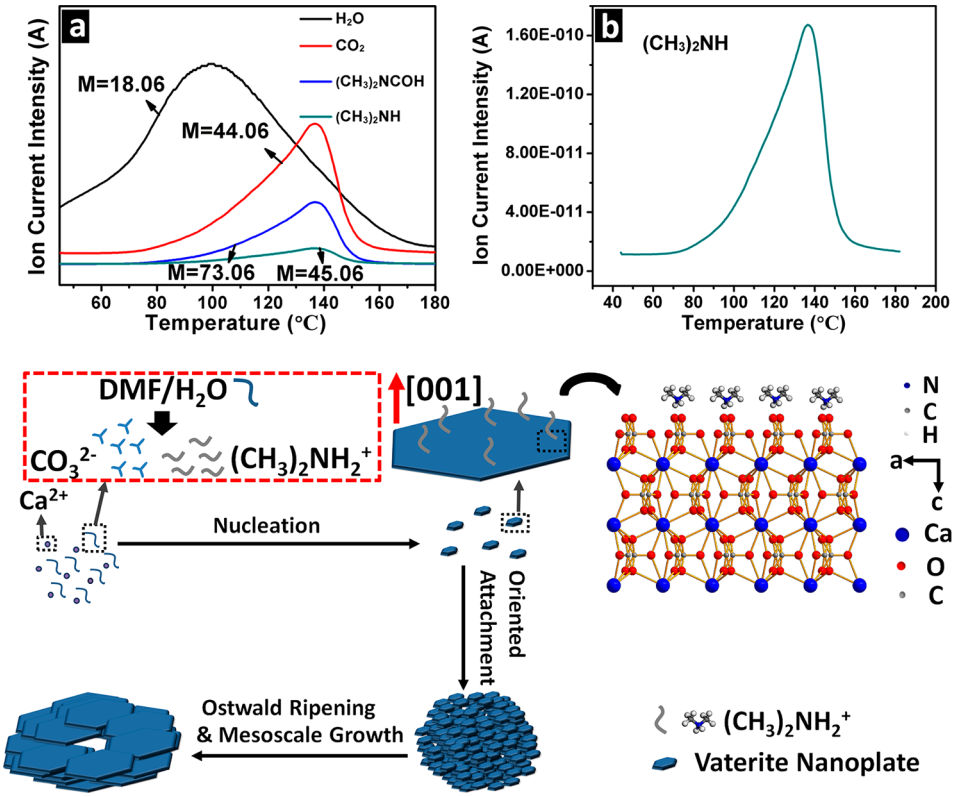

Figure 2. (a) TG-DSC and (b) TG-MS curves of DMF/H_2O (3:1 v/v) mixed solvent at temperature ranging from 40 to 180 °C. The schematic illustration presents the tentative formation mechanism of the vaterite $CaCO_3$ nanoplate assemblies with exposed {001} facets, where the positively charged dimethylamine ions ($(CH_3)_2NH_2^+$) bond with the carbonate ions via electrostatic interaction, stabilizing and promoting the {001} facets of vaterite in the final product.

demonstrated to stabilize and inhibit {001} facets of vaterite.[24−26] Herein, combined with the solvent effects of the mixed solvents (DMF-H_2O), the in situ produced positively charged $(CH_3)_2NH_2^+$ ions are proposed to adsorb onto {001} facets of vaterite, stabilizing and directing the formation of the exposed {001} facets. To the best of our knowledge, it is a novel strategy to utilize DMF-H_2O solvothermal reactions to synthesize carbonates, quite apart from its familiar functions in previous work as mere solvent or reducing reagent.[27,28]

The products are formed via an aggregation-mediated process, as shown in Figure S3. After 2 h, the primary round cakelike particles consisted of vaterite nanoparticles formed. The particles have an average diameter of 1 μm, indicating that the initially formed nanoparticles aggregated orientedly (Figure S3a, b). As time was prolonged to 4 h, the nanoparticles of the round cakelike particles encountered a series of mesoscale growth process, involving the hollowing of the central district, and the crystallographic fusion of the vaterite nanoparticles, due to the Ostwald ripening (Figure S3c, d). As indicated by the red arrows in Figure S3d, the nanoparticle around the central district of the particles had a slower crystallographic fusion process than those in the districts outside, as may be caused by the more sufficient reaction ions around the particle than in the central district. The matured product was formed after reaction for 6 h, as indicated by the red arrows in Figure S3e, f, the nanoparticles in the central district almost disappear, indicating a further crystallographic fusion process in the final product. The tentative formation mechanism of the product is illustrated in Figure 2. The particle size of the product can be controlled by altering the reaction temperatures, and the reaction time. In this regard, a variety of similar products with diameters ranging from 0.8 to 1.9 μm can be achieved at 100−140 °C for 4−8 h (Figure S4). The particle size increases while the reaction temperature rises, which is attributed to the increased reaction ions mobility, and the increased concentration of the in situ $(CH_3)_2NH_2^+$ ions at elevated temperature, resulting in an enhanced effect on forming the {001} high energy facets, and thus the increase of the particle size. We wish to highlight that this work presents us an example on reworking and exploring an earlier binary-solvent system for synthesizing calcium carbonate by reaction-assisted synthetic protocols without additives.

To evaluate the performance of the sample as an inorganic vehicle, we tried different weight ratios of DOX to $CaCO_3$ in order to obtain the maximum drug-loading capacity. Interestingly, as shown in Figure 3a, the sample has a maximum drug-loading capacity up to 65% and a high encapsulation efficiency of around 80%. To the best of our knowledge, the maximum drug-loading capacity of our sample is nearly 8 times greater than the best of previous $CaCO_3$-based vehicles (that proved effective in cell cytotoxicity tests),[11−14] and is even comparable to SWCNTs loaded at normal PH (68%).[29] Statistical data of the performance of a variety of inorganic vehicles is presented in Table S1, part of which are shown as bar chart for visualization in Figure 3b. The high drug-loading capacity renders our product an appealing host for DDS.

The drug-release profiles of the $CaCO_3$-DOX delivery system are presented in Figure 3c. First, our product has an admirable PH-sensitivity with extremely low drug release (<10% at pH 7.4) at simulated physiological condition, and 80% release at pH 4 over 216 h, as illustrated by the dramatic change from opaque

DOI: 10.1021/acsami.5b04819
ACS Appl. Mater. Interfaces 2015, 7, 15686−15691

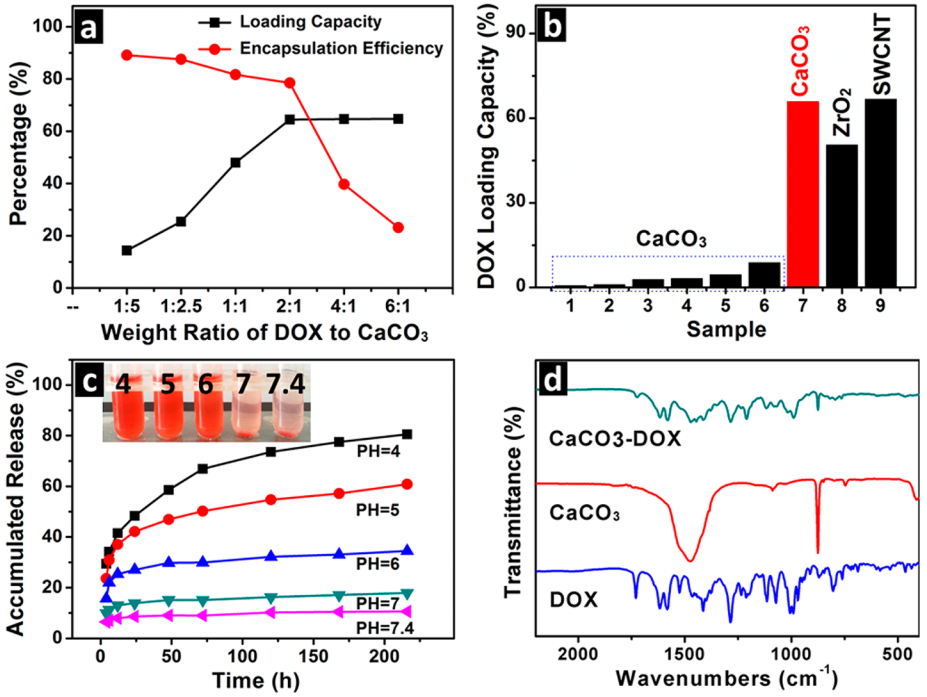

Figure 3. (a) DOX loading capacity and encapsulation efficiency of the samples at different weight ratios of DOX to $CaCO_3$. (b) Statistical bar chart of DOX loading capacity of diverse inorganic-based vehicles. The red bar represents data of our work, whereas black bars represent those of other work.[4,11−13,29] (c) Releasing profile of the $CaCO_3$-DOX delivery system at pH 4.0, 5.0, 6.0, 7.0, and 7.5. (d) FT-IR spectra of the free DOX, bare $CaCO_3$, and $CaCO_3$-DOX.

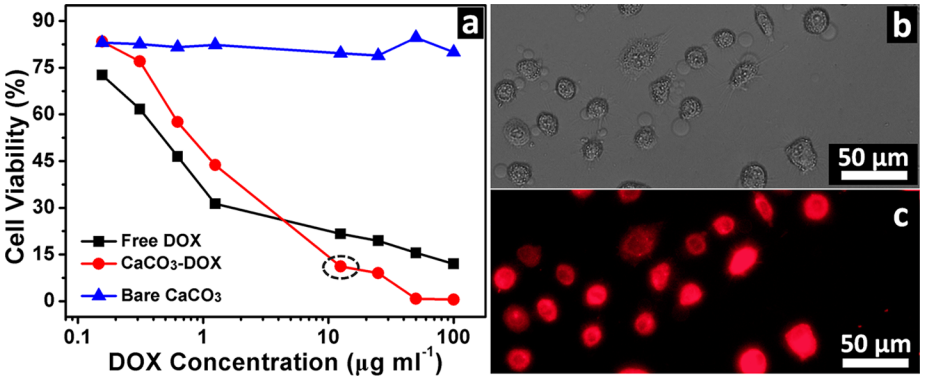

Figure 4. (a) Survival of HepG2 cells in various concentrations of the bare $CaCO_3$, free DOX, and $CaCO_3$-DOX after incubation with cells for 48 h. (the performance of the bare $CaCO_3$ is presented herein for visualization, though the *x*-axis is the $CaCO_3$ concentration indeed) (b) Optical image, and (c) fluorescent image of the HepG2 cells treated with $CaCO_3$- DOX of 12.5 μg/mL for 48 h.

red at pH 4 to near-translucent light at pH 7 (inset in Figure 3c). Furthermore, compared to previous work, the initial burst release appears to be inherently quite well inhibited in acidic conditions, as evidenced by no more than 30% release within the first 4 h at pH 4−6. More importantly, sustainable release responses are realized at acidic conditions, as can be seen that a long period of 216 h is required to release 80% of the total DOX molecules at pH 4. Key release parameters of diverse inorganic-based DDSs are presented in Table S2. Actually, we envision that the inhibition of initial burst release and the behavior of subsequent sustainable releasing are both considered favorable for cancer cure as such a pattern causes less shock to a patient's body, as well as prolongs the drug efficacy and decreases the drug uptake frequency, which might be particularly beneficial for elderly patients and children.

As most earlier systems have much larger specific surface area than our product (Figure S5, 21 $m^2\ g^{-1}$),[4,8,9,13,16] in particular, single-walled carbon nanotubes with a theoretical specific surface area up to 2600 $m^2\ g^{-1}$,[29] we speculate that the intrinsic nature of the crystal structure, especially the surface structure, is the dominant factor for our good results in the DOX loading and releasing, which has been proposed as one important factor for the high drug-loading of calcium silicate hydrate in previous work.[9] First, to eliminate the effects caused by the small amount of the organic residues, we tested the loading capacity of the annealed sample with the organic residues completely removed. As can be seen in Figures S6 and S7, the annealed sample showed comparable DOX loading capacity as to the unannealed sample, which indicates that, the small amount of organic residues left in the product make negligible contribution to the drug loading. The FT-IR spectrum (Figure 3d) of the $CaCO_3$-DOX displays characteristic bands of DOX and $CaCO_3$ without obvious band shift or loss, confirming the DOX immobilization on $CaCO_3$ without prominent structural transformation, and

DOI: 10.1021/acsami.5b04819
ACS Appl. Mater. Interfaces 2015, 7, 15686−15691

also the electrostatic interaction between DOX and $CaCO_3$ as the dominant force. Herein, the $-NH_2^+$ groups of the DOX molecules are proposed to link with the CO_3^{2-} anions of the {001} facets via the electrostatic bonding, similar to the electrostatic interaction between $-COO^-$ groups of the ibuprofen molecules (another type of drug molecule) and the Ca^{2+} cations of the surface of the calcium silicate hydrate reported by Zhu *etc.*[9] The photoluminescence of the $CaCO_3$-DOX (Figure S8) is quenched to a certain extent, a phenomenon which has already been observed in zirconia nanocapsules/DOX and carbon nanotubes/DOX;[4,29] however, it has not been reported in a $CaCO_3$-based DDS. It is another evidence of interactions between the loaded DOX molecules and the $CaCO_3$ crystal surfaces. Thus, it is bold to speculate that the high drug loading and the sustaining of subsequent releasing behavior may be probably ascribed to the crystal facet−drug molecule interactions at the atomic or molecular level.

The 48 h 3-(4,5-dimethylthiazol-2-yl)-2,5-diphenyltetrazolium bromide (MTT) in vitro cell cytotoxicity experiment was conducted to further evaluate the drug efficacy of the $CaCO_3$-DOX. As shown in Figure 4a, the bare $CaCO_3$ does not show distinct cytotoxicity to HepG2 cells, demonstrating its good biocompatibility. After conjugating DOX molecules, the $CaCO_3$-DOX shows prominent dose-dependent cytotoxicity toward HepG2 cells, demonstrating the drug efficacy of the $CaCO_3$-DOX, which is similar to the result of previous work.[11] At appropriate concentrations ($c > 10\ \mu g\ mL^{-1}$), the $CaCO_3$-DOX shows enhanced cell cytotoxicity toward HepG2 cells than free DOX. However, considering the release of less than 60% within 48 h and the prolonged releasing time afterward (Figure 3c), the long-term drug efficacy of our DDS may be anticipated. As shown by the images in Figure 4b, c, the HepG2 cells are round and bear bubbles inside, indicating the cell death, and the DOX-induced cell death is confirmed by the strong red fluorescence emission of the HepG2 cells after coincubating with $CaCO_3$-DOX ($12.5\ \mu g\ mL^{-1}$) for 48 h.

In summary, vaterte $CaCO_3$ nanoplate assemblies with substantially exposed {001} high-energy facets are synthesized via a novel, additive-free strategy in DMF/H_2O. A maximum DOX-loading capacity up to 65% is achieved, rivaling all the $CaCO_3$-based DDSs so far. Moreover, the product's sustainable release behavior and the inhibition of initial burst release endow it with long-term chemotherapeutic efficacy. The work develops a new way of additive-free strategy toward vaterite $CaCO_3$ nanoplate assemblies with exposed high-energy {001} facets, and more importantly, it highlights the crystal surface structure and chemistry at atomic level for rational design of a DDS with high drug-loading capacity and sustainable-releasing behavior.

■ ASSOCIATED CONTENT

Supporting Information

The experimental section, the supplementary characterization of the product, the intermediate at the initial stage, and the table of performances on different inorganic-based drug carriers. The Supporting Information is available free of charge on the ACS Publications website at DOI: 10.1021/acsami.5b04819.

■ AUTHOR INFORMATION

Corresponding Author

*E-mail: zyfu@whut.edu.cn. Phone: 86-027- 87662983.

Author Contributions

The manuscript was written through contributions of all authors. All authors have given approval to the final version of the manuscript.

Notes

The authors declare no competing financial interest.

■ ACKNOWLEDGMENTS

This work was financially supported by the National Natural Science Foundation of China (51161140399) and the Ministry of Science and Technology of China (2015DFR50650). Y.L. acknowledges Hubei Provincial Department of Education for the "Chutian Scholar" program. B.-L.S. acknowledges a program for Changjiang Scholars and Innovative Research Team (IRT1169)

■ ABBREVIATIONS

DDS, drug delivery system
DMF, dimethylformamide

■ REFERENCES

(1) Langer, R. Drug Delivery and Targeting. *Nature* **1998**, *392*, 5−10.
(2) Ferrari, M. Cancer Nanotechnology: Opportunities and Challenges. *Nat. Rev. Cancer* **2005**, *5*, 161−171.
(3) Niu, D. C.; Liu, Z. J.; Li, Y. S.; Luo, X. F.; Zhang, J. Y.; Gong, J. P.; Shi, J. L. Monodispersed and Ordered Large-Pore Mesoporous Silica Nanospheres with Tunable Pore Structure for Magnetic Functionalization and Gene Delivery. *Adv. Mater.* **2014**, *26*, 4947−4953.
(4) Tang, S.; Huang, X.; Chen, X.; Zheng, N. Hollow Mesoporous Zirconia Nanocapsules for Drug Delivery. *Adv. Funct. Mater.* **2010**, *20*, 2442−2447.
(5) Oh, J. M.; Choi, S. J.; Lee, G. E.; Han, S. H.; Choy, J. H. Inorganic Drug-Delivery Nanovehicle Conjugated with Cancer-Cell-Specific Ligand. *Adv. Funct. Mater.* **2009**, *19*, 1617−1624.
(6) Peng, F.; Su, Y.; Wei, X.; Lu, Y.; Zhou, Y.; Zhong, Y.; Lee, S. T.; He, Y. Silicon-Nanowire-Based Nanocarriers with Ultrahigh Drug-Loading Capacity for In Vitro and In Vivo Cancer Therapy. *Angew. Chem., Int. Ed.* **2013**, *52*, 1457−1461.
(7) Chen, Y.; Chen, H. R.; Zeng, D. P.; Tian, Y. B.; Chen, F.; Feng, J. W.; Shi, J. L. Core/Shell Structured Hollow Mesoporous Nanocapsules: A Potential Platform for Simultaneous Cell Imaging and Anticancer Drug Delivery. *ACS Nano* **2010**, *4*, 6001−6013.
(8) Du, X.; Shi, B. Y.; Liang, J.; Bi, J. X.; Dai, S.; Qiao, S. Z. Developing Functionalized Dendrimer-Like Silica Nanoparticles with Hierarchical Pores as Advanced Delivery Nanocarriers. *Adv. Mater.* **2013**, *25*, 5981−5985.
(9) Wu, J.; Zhu, Y. J.; Cao, S. W.; Chen, F. Hierachically Nanostructured Mesoporous Spheres of Calcium Silicate Hydrate: Surfactant-Free Sonochemical Synthesis and Drug-Delivery System with Ultrahigh Drug-Loading Capacity. *Adv. Mater.* **2010**, *22*, 749−753.
(10) Yang, J. H.; Han, Y. S.; Park, M.; Park, T.; Hwang, S. J.; Choy, J. H. New Inorganic-based Drug Delivery System of Indole-3-acetic Acid-layered Metal Hydroxide Nanohybrids with Controlled Release rate. *Chem. Mater.* **2007**, *19*, 2679−2685.
(11) Wei, W.; Ma, G. H.; Hu, G.; Yu, D.; McLeish, T.; Su, Z. G.; Shen, Z. Y. Preparation of Hierarchical Hollow $CaCO_3$ Particles and the Application as Anticancer Drug Carrier. *J. Am. Chem. Soc.* **2008**, *130*, 15808−15810.
(12) Zhao, Y.; Lu, Y.; Hu, Y.; Li, J. P.; Dong, L. A.; Lin, L. N.; Yu, S. H. Synthesis of Superparamagnetic $CaCO_3$ Mesocrystals for Multistage Delivery in Cancer Therapy. *Small* **2010**, *6*, 2436−2442.
(13) Guo, Y. M.; Zhang, J.; Jiang, L. L.; Shi, X. M.; Yang, L.; Fang, Q. L.; Fang, H.; Wang, K.; Jiang, K. Facile One-pot Preparation of Calcite Mesoporous Carrier for Sustained and Targeted Drug Release for Cancer Cells. *Chem. Commun.* **2012**, *48*, 10636−10638.

DOI: 10.1021/acsami.5b04819
ACS Appl. Mater. Interfaces 2015, 7, 15686−15691

(14) Wang, J.; Chen, J. S.; Zong, J. Y.; Zhao, D.; Li, F.; Zhuo, R. X.; Cheng, S. X. Calcium Carbonate/Carboxymethyl Chitosan Hybrid Microspheres and Nanospheres for Drug Delivery. *J. Phys. Chem. C* **2010**, *114*, 18940−18945.
(15) Wang, F.; Pauletti, G. M.; Wang, J.; Zhang, J.; Ewing, R. C.; Wang, Y.; Shi, D. Dual Surface-Functionalized Janus Nanocomposites of Polystyrene/Fe3O4@SiO2 for Simultaneous Tumor Cell Targeting and Stimulus-Induced Drug Release. *Adv. Mater.* **2013**, *25*, 3485−3489.
(16) Li, D.; Tang, J.; Wei, C.; Guo, J.; Wang, S. L.; Chaudhary, D.; Wang, C. C. Doxorubicin-Conjugated Mesoporous Magnetic Colloidal Nanocrystal Clusters Stabilized by Polysaccharide as a Smart Anticancer Drug Vehicle. *Small* **2012**, *8*, 2690−2697.
(17) Tian, N.; Zhou, Z. Y.; Sun, S. G.; Ding, Y.; Wang, Z. L. Synthesis of Tetrahexahedral Platinum Nanocrystals with High-index Facets and High Electro-oxidation Activity. *Science* **2007**, *316*, 732−735.
(18) Vallet-Regí, M.; Balas, F.; Arcos, D. Mesoporous Materials for Drug Delivery. *Angew. Chem., Int. Ed.* **2007**, *46*, 7548−7558.
(19) Hoffmann, F.; Cornelius, M.; Morell, J.; Fröba, M. Silica-Based Mesoporous Organic−Inorganic Hybrid Materials. *Angew. Chem., Int. Ed.* **2006**, *45*, 3216−3251.
(20) Pinna, N.; Niederberger, M. Surfactant-free Nonaqueous Synthesis of Metal Oxide Nanostructures. *Angew. Chem., Int. Ed.* **2008**, *47*, 5292−5304.
(21) Gebauer, D.; Coelfen, H.; Verch, A.; Antonietti, M. The Multiple Roles of Additives in $CaCO_3$ Crystallization: A Quantitative Case Study. *Adv. Mater.* **2009**, *21*, 435−439.
(22) Orme, C. A.; Noy, A.; Wierzbicki, A.; McBride, M. T.; Grantham, M.; Teng, H. H.; Dove, P. M.; DeYoreo, J. J. Formation of Chiral Morphologies through Selective Binding of Amino Acids to Calcite Surface Steps. *Nature* **2001**, *411*, 775−779.
(23) Volodkin, D. V.; Larionova, N. I.; Sukhorukov, G. B. Protein Encapsulation via Porous $CaCO_3$ Microparticles Templating. *Biomacromolecules* **2004**, *5*, 1962−1972.
(24) Xu, A. W.; Antonietti, M.; Cölfen, H.; Fang, Y. P. Uniform Hexagonal Plates of Vaterite $CaCO_3$ Mesocrystals Formed by Biomimetic Mineralization. *Adv. Funct. Mater.* **2006**, *16*, 903−908.
(25) Pouget, E. M.; Bomans, P. H. H.; Dey, A.; Frederik, P. M.; de With, G.; Sommerdijk, N. A. J. M. The Development of Morphology and Structure in Hexagonal Vaterite. *J. Am. Chem. Soc.* **2010**, *132*, 11560−11565.
(26) Mann, S.; Heywood, B. R.; Rajam, S.; Birchall, J. D. Controlled Crystallization of $CaCO_3$ under Stearic Acid Monolayers. *Nature* **1988**, *334*, 692−695.
(27) Guo, X. H.; Yu, S. H.; Cai, G. B. Crystallization in a Mixture of Solvents by Using a Crystal Modifier: Morphology Control in the Synthesis of Highly Monodisperse $CaCO_3$ Microspheres. *Angew. Chem., Int. Ed.* **2006**, *45*, 3977−3981.
(28) Carpenter, M. K.; Moylan, T. E.; Kukreja, R. S.; Atwan, M. H.; Tessema, M. M. Solvothermal Synthesis of Platinum Alloy Nanoparticles for Oxygen Reduction Electrocatalysis. *J. Am. Chem. Soc.* **2012**, *134*, 8535−8542.
(29) Liu, Z.; Sun, X. M.; Nakayama-Ratchford, N.; Dai, H. J. Supramolecular Chemistry on Water-soluble Carbon Nanotubes for Drug Loading and Delivery. *ACS Nano* **2007**, *1*, 50−56.

DOI: 10.1021/acsami.5b04819
ACS Appl. Mater. Interfaces 2015, 7, 15686−15691